ACS Macro Letters

Letter

pubs.acs.org/macroletters

Simulation of Defect Reduction in Block Copolymer Thin Films by Solvent Annealing

Su-Mi Hur,[†,‡] Gurdaman S. Khaira,[†] Abelardo Ramírez-Hernández,[†,‡] Marcus Müller,[§] Paul F. Nealey,[†,‡] and Juan J. de Pablo*[,†,‡]

[†]Materials Science Division, Argonne National Laboratory, 9700 South Cass Avenue, Argonne, Illinois 60439, United States

[‡]Institute for Molecular Engineering, The University of Chicago, Chicago, Illinois 60637, United States

[§]Institut für Theoretische Physik, Georg-August-Universität, 37077 Göttingen, Germany

Supporting Information

ABSTRACT: Solvent annealing provides an effective means to control the self-assembly of block copolymer (BCP) thin films. Multiple effects, including swelling, shrinkage, and morphological transitions, act in concert to yield ordered or disordered structures. The current understanding of these processes is limited; by relying on a theoretically informed coarse-grained model of block copolymers, a conceptual framework is presented that permits prediction and rationalization of experimentally observed behaviors. Through proper selection of several process conditions, it is shown that a narrow window of solvent pressures exists over which one can direct a BCP material to form well-ordered, defect-free structures.

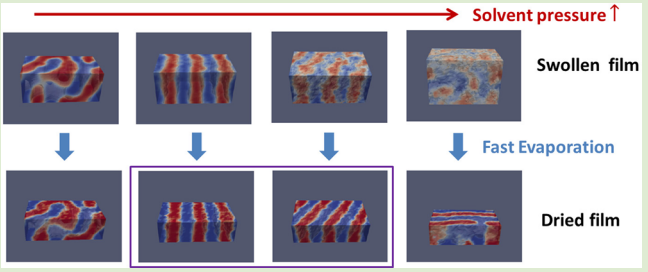

Ordered domains in BCPs have characteristic length scales in the 5 to 50 nm range. Such a range is commensurate with the smallest features encountered in semiconductor devices, nanofluidic devices, or high-density storage media, where lithographic approaches based on directed BCP self-assembly could be advantageous.[1,2] In general, BCP thin films are prepared by spin-casting a polymer solution onto a substrate, leading to poorly defined structures riddled with defects. Thermal annealing,[3] solvent annealing,[4−11] or external fields (e.g., shear)[12,13] can all be used to reduce defect density. Solvent annealing of spun-cast BCP thin films is carried out under a solvent atmosphere, usually at room temperature, thereby swelling the material and changing its characteristics. Solvents also increase mobility and facilitate the reorganization of a self-assembled film into a well-ordered structure. Lower processing temperatures decrease the risk of thermal degradation and could enable the use of BCPs of greater chemical diversity.[14]

It has been proposed that highly incompatible copolymers (such as PS-*b*-PDMS) facilitate formation of ordered structures over large areas.[4,5] BCPs with high χ (where χ denotes the Flory−Huggins parameter that quantifies the segregation force between distinct polymer segments) exhibit a larger thermodynamic driving force for microphase separation and, the argument goes, have a higher driving force for reducing the defect population. Recent work has shown, however, that even for low-χ diblock copolymers the free energy of defects in directed self-assembly is extremely large, on the order of hundreds of k_BT because many polymer molecules participate in forming the defect.[15,16] The equilibrium probability of forming a defect is therefore vanishingly small. Thermodynamics, then, is not enough to explain the large density of defects that is sometimes encountered in experiments. Such results reinforce the view that the defects observed in BCP films represent kinetically trapped, nonequilibrium structures. Indeed, in this work we use theory and simulations to dispel the notion that a high-χ material is essential to achieve low defectivity; we propose instead that solvent annealing improves directed self-assembly (DSA) by lowering the kinetic barriers that impede defect annihilation in neat samples, thereby providing an effective strategy for creation of defect-free self-assembled BCP films over large areas.

Most theoretical and computational studies of BCP DSA have not considered the process of annealing and the underlying kinetics, and only recently have efforts been made on these.[17,18] By using a substantially different approach from previous works, we describe that process by relying on a theoretically informed coarse-grained (TICG) model that enables study of not only the equilibrium phase behavior of solvated BCPs, but also the kinetics of microphase separation. Such a model has been shown to provide a reliable description of BCP melts in thin films.[19−21] Here, it is modified by introducing a generalized energy functional expansion in terms of number densities up to third order,[22,23] as opposed to the original binary Flory−Huggins interaction terms used in

Received: November 5, 2014
Accepted: November 26, 2014
Published: December 11, 2014

   dx.doi.org/10.1021/mz500705q | *ACS Macro Lett.* 2015, 4, 11−15

previous work. The model is thus able to predict liquid−vapor equilibria, and the evaporation or sorption of a solvent into a polymer film.[23] In the Supporting Information, we briefly recount the model and how its parameters are chosen to simulate thin polymer films in equilibrium with a vapor. Our simulation approach is also designed to describe the time evolution of microphase separation and, as such, the polymer chain mobility depends on composition (solvent concentration).

As a reference system, we consider a symmetric A-*b*-B BCP that corresponds to a 40k-40k PS-*b*-P2VP copolymer. We use $N = 32$ interaction sites to model our polymer chains. For simplicity, the solvent, which is representative of acetone, is chosen to be good and nonselective for either polymer block. Initially, a poorly ordered dry BCP film is prepared by fast evaporation of solvent particles from an equilibrated dilute BCP film (Figure 1a). The film thickness of the dry film is $2R_e$. Here

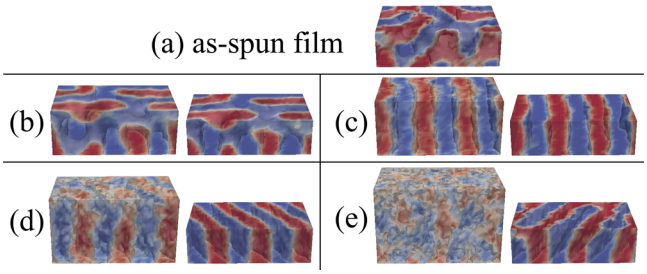

Figure 1. Self-assembly of symmetric BCP thin films of $\chi_{AB}N = 50$ after swelling (left) and after solvent evaporation (right). As-spun configurations (a) are swollen under various solvent pressures. The polymer compositions ϕ_p are therefore different ($\phi_p = 0.8$, 0.7, 0.6, and 0.5 for (b), (c), (d), and (e), respectively). Right hand side images show the morphologies obtained after the solvent particles are removed from the swollen films.

R_e is the average end-to-end distance of polymer chains in the melt. In experimental annealing processes a sample is placed in a solvent annealing chamber for a certain amount of time, which is generally longer than that required for the film to swell and reach a steady-state concentration. That process is replicated in simulations by adding solvent particles above the polymer film, and conducting annealing simulations for a preset amount of time. The total annealing time employed here corresponds to the time required by a homopolymer molecule to diffuse a mean square displacement of $25R_e^2$ in a system that contains a polymer volume fraction of $\phi_p = 0.9$. Different solvent pressures lead to different polymer volume fractions ϕ_p in the swollen state; smaller values of ϕ_p correspond to larger solvent pressures. Representative morphologies of swollen copolymer thin films are shown in Figure 1 for $\phi_p = 0.8$, 0.7, 0.6, and 0.5. After swelling, solvent evaporation is implemented by removing solvent particles from the vapor phase at a fixed rate; less than one tenth of the annealing time is required to remove more than 99% of the solvent from the swollen film at $\phi_p = 0.5$.[24] Figure 1 also shows the resulting morphologies after the solvent is removed. When $\phi_p = 0.8$, the amount of solvent in the swollen film is not sufficient to enhance polymer chain mobility and remove defects from the as-spun film. The swollen film morphology, therefore, continues to exhibit kinetically trapped defects (Figure 1b). Since solvent particles are removed fast, the dry film on the right-hand side shows a configuration that is similar, except that it has shrunk in the direction normal to the substrate. In contrast, when ϕ_p is too low, the BCP enters the disordered swollen state and a defective dried film is observed after removing the solvent (Figure 1e).

The dilution of unfavorable interactions between dissimilar blocks by a solvent was first discussed by Helfand and Tagami.[25,26] Past studies have shown that copolymers follow a general expression of the form $\chi_{eff} = \phi_p^{\alpha}\chi_{AB}$, with a scaling exponent α in the range of 1.0 to 1.6.[27−33] As ϕ_p becomes smaller an order−disorder phase transition occurs.[28,34,35] When the solvent is evaporated at a fast rate from a disordered swollen film, the system re-enters the ordered phase rapidly, and the final dry film exhibits defective lamellae, as shown in the right panel of Figure 1e. At intermediate concentrations ($\phi_p = 0.7$ and 0.6), however, defects in the film are removed during the swelling process; the dry film is therefore free of defects (Figure 1c,d). The observed ordering process is reminiscent of the self-seeding technique for the growth of single crystals of polymers, where noncomplete melting leaves behind an initial seed that enables generation of arrays of orientation-correlated polymer crystals of uniform size and shape.[36,37] A noteworthy feature of the dry films is that the domain spacing of lamellae at $\phi_p = 0.6$ is smaller than that observed at $\phi_p = 0.7$; this is due to the fact that $\chi_{eff}N$ is smaller in the former case. The lamellae adopt a tilted orientation to adjust to the smaller domain size under the constraints imposed by a fixed-size simulation box. The dry films exhibit similar configurations to those of the original swollen films, in terms of the domain size and location of the AB interfaces. Consistent with recent experimental observations,[8,38] the final morphologies obtained in solvent annealing do not correspond to equilibrium but, in fact, represent nonequilibrium states that are inherited from the swollen films.

In Figure 2 we show results from solvent annealing simulations for different $\chi_{AB}N$ at various concentrations. First, we consider the case where only χ_{AB} is varied, while N is kept constant at $N = 32$. As χ_{AB} becomes larger, the window for defect removal by solvent addition is shifted toward higher solvent concentrations, and the corresponding domain size increases due to the higher $\chi_{eff}N$. A disordered phase is

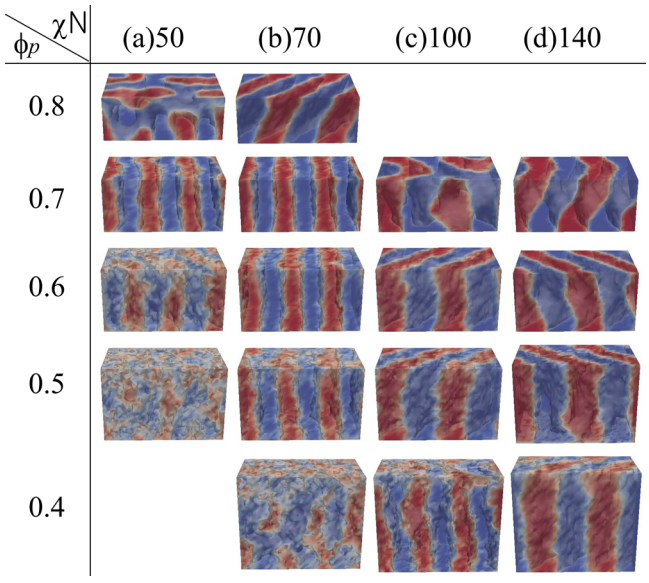

Figure 2. Morphologies of swollen films at various ϕ_p for different $\chi_{AB}N$ for $N = 32$.

dx.doi.org/10.1021/mz500705q | ACS Macro Lett. 2015, 4, 11−15

observed at smaller ϕ_p. Figure 3 shows results for polymers with half the molecular weight (N = 16) of that considered in

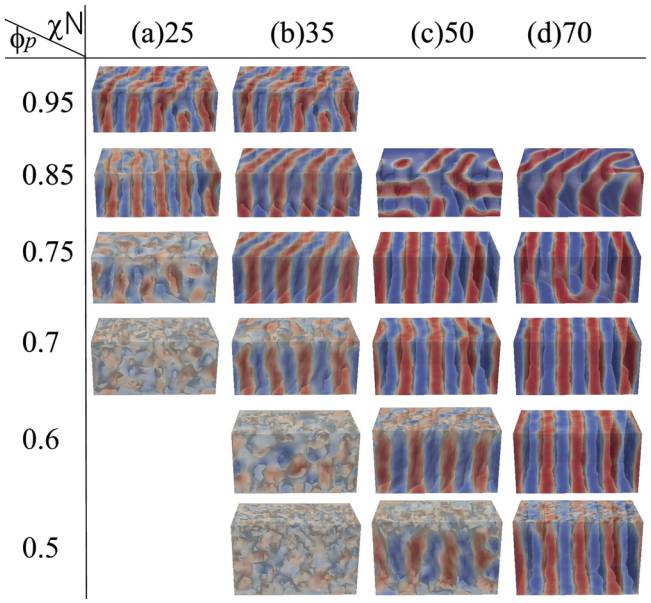

Figure 3. Morphologies of swollen films at various ϕ_p for different $\chi_{AB}N$ for N = 16.

Figure 2 but having the same χ_{AB}. For the shorter chains, domain sizes are smaller and the line-edge roughness at the interface is more pronounced.

The range of solvent concentrations over which defect-free structures are observed shifts significantly depending on the material and process characteristics. As mentioned earlier, $\chi_{eff} = \phi_p^{\alpha} \chi_{AB}$. In semidilute BCP solutions in nonselective good solvents, α is predicted to be 1.6.[31−33] This value of α has been confirmed experimentally, even for concentrated systems, in solutions of nearly symmetric PS-*b*-PI copolymers in a neutral good solvent.[27,28] Note that deviations of α from the dilute approximation (α = 1) are attributed to increases of the excluded volume screening length. In simulations with a small degree of discretization N, however, it is difficult to capture the reduction of intermolecular contacts due to the increase of the excluded volume screening length upon solvent addition. It is therefore difficult to attain the asymptotic value of exponent α[39] expected for semidilute or concentrated systems. Indeed, as shown in the Supporting Information, we observe α = 1 for our systems and we plot $\chi_{eff}N$ as a function of ϕ_p using that exponent for all simulations shown in Figure 4. Solid and dashed lines correspond to polymer systems with N = 32 and 16, respectively. Note that Figures 2a and 3c, and Figures 2b and 3d have the same $\chi_{AB}N$, and the corresponding curves overlap each other. Red dots, black triangles, and black squares correspond to simulations in which defect-free, disordered, and defective swollen morphologies were obtained, respectively. Multiple simulations were carried out for each parameter set; to determine morphologies near the boundary, 10 independent simulations were conducted under the same conditions, and the most probable morphology was entered in the figure. There exist a lower limit of ϕ_p above which defect-free morphologies are observed; below that limit, one cannot generate an ordered phase in a swollen film. We expect this limit of ϕ_p to correspond to χN_{ODT}. For symmetric BCPs, mean field theory predicts $(\chi N)_{ODT}$ = 10.495.[40] The model considered here

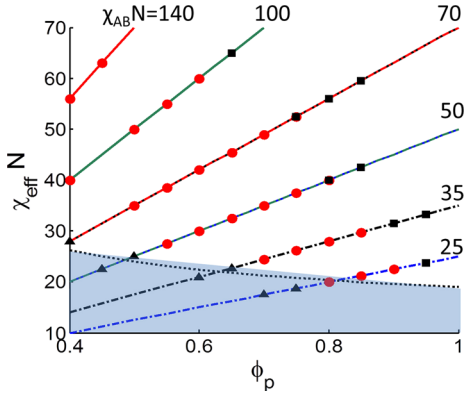

Figure 4. $\chi_{eff}N = \phi_p\chi_{AB}N$ as a function of ϕ_p for different BCP systems. Blue, black, green, and red solid lines correspond to $\chi_{AB}N$ = 50, 70, 100, and 140, respectively. Dashed lines correspond to cases with half molecular weights and half χN. Red dots are simulation data points where defect-free morphologies were obtained. The black dotted curve shows the function $\chi_{eff}N = 10.495 + c_2\phi_p^{-2/3}$, and it delineates the lower limit of $\chi_{eff}N$, above which an ordered phase is expected to form when fluctuations are incorporated in the model.

includes fluctuations, and the ODT is therefore expected to be higher than that predicted from a mean-field approximation. Furthermore, the value of χN_{ODT} is also expected to depend on ϕ_p. In Figure 4, we plot the function $\chi_{eff}N_{ODT} = 10.495 + c_2\phi_p^{-2/3}$, taken from the Fredrickson−Helfand formula for the shift of the ODT in bulk BCP systems.[41] The coefficient c_2 is estimated to be 10.7093 for N = 32, in close agreement with an earlier study of the ODT for the model considered here in the absence of a solvent.[19]

In contrast to the lower bound identified above, no obvious trend is immediately apparent for an upper bound in Figure 4. To define an upper ϕ_p bound, we adopt the view that defect annihilation as an activated process and determine the corresponding kinetic-barrier heights, ΔF_b. Using a Kramers-like approach, we assume that the average time τ for defect annihilation is proportional to exp $[\Delta F_b/kT]$ for $\Delta F_b \gg kT$, which has been confirmed in experiments of the temperature-dependence of the rate of defect annihilation.[3] When this characteristic time τ is smaller than a given annealing time, the annealing process should remove most defects in the film. In practice, this annealing time cannot be too long, due to dewetting of thin polymer films (this process will depend on the characteristics of the underlying polymer brush or substrate). A short annealing time is also desirable from a purely practical point of view. A defect annihilation time τ can be estimated according to $\zeta^2 \exp(a\phi_p\chi_{AB}N)/D_0$, where we have assumed a linear relationship between ΔF_b and $\chi_{eff}N$;[15,42] ζ is the characteristic length scale of the defects. The diffusivity $D_0(\phi_p,N)$ of a polymer chain at the same concentration is determined from bulk simulations at different ϕ_p and N. Our results indicate that a = 0.025. Note that free-energy calculations aimed at deriving the exact relationship between ΔF_b and $\chi_{eff}N$ (and N) are currently under way; at this point, we view it as a reasonable approximation based on available experimental evidence from diffusivity measurements.[43] Also note that a constant shift, β, is expected in the linear relationship between ΔF_b and $\chi_{eff}N$ because a nonzero positive $\chi_{eff}N$ should exist where defective structures are unstable. In our analysis, this constant is ignored and τ is actually rescaled by $1/(\zeta^2 \exp \beta)$. Precise estimates for the defect annihilation time

dx.doi.org/10.1021/mz500705q | ACS Macro Lett. 2015, 4, 11−15

can be produced once this shift is obtained from different sets of simulations for a detailed free energy landscape.

The phenomenological description of defect-annihilation times τ for the systems considered here are plotted as a function of ϕ_p along with simulation results in Figure 5. A horizontal dotted line (black) is drawn at τ^* to delineate the upper limit of ϕ_p that leads to defect-free structures for the annealing time considered here.[44] For a given polymer, the defect annihilation time is found to be highly sensitive to ϕ_p. A rapid decrease of τ as ϕ_p decreases is observed due to the combined effect of a reduced F_b and an increased D_0. Such a decrease helps explain recent experimental observations of larger ordered grain sizes at higher solvent pressures.[38] For BCPs with a large segregation strength, the curve is shifted upward considerably, due to the larger barrier heights F_b for large $\chi_{eff}N$ materials. Therefore, at a fixed solvent pressure, large χN polymers are less likely to form defect-free structures; this result goes against the argument that BCPs with high $\chi_{AB}N$ are advantageous for defect reduction.[4,5] When the molecular weight is reduced, the τ curve is shifted downward due to an increased polymer chain mobility. The lower limit of ϕ_p is determined mainly by $\chi_{eff}N$ and, therefore, curves corresponding to Figures 2a and 3c and Figures 2b and 3d exhibit a similar lower boundary. However, the characteristic times τ for shorter chains (dotted lines) are smaller, leading to higher upper boundaries (the ϕ_p where the τ curve crosses τ^*). The process window for defect removal in a short polymer having a higher χ_{AB} is therefore wider than that of a material having the same $\chi_{AB}N$ but a higher molecular weight.

We conclude our discussion by emphasizing the importance of kinetic pathways in solvent annealing. Specifically, instead of swelling an as-spun film directly up to a specific value of ϕ_p (Figure 1), we propose that a two-step evaporation procedure be carried out in which the film is first swollen into a disordered state under high solvent pressure, and then a fraction of the solvent is removed until the desired swelling ratio (ϕ_p) is attained. This two-step approach yields a well-controlled and highly reproducible starting state; it decouples the parameters of the spin-casting, and, therefore, widens the window for defect removal to higher ϕ_p (Figure 6). By starting the ordering process from a disordered state, rather than from a defect-riddled state, and holding the system for a period of time at a ϕ_p above ϕ_{ODT}, local defects are removed efficiently, leading to well-ordered swollen morphologies (Figure 6a–c), even for the higher ϕ_p (Figure 6c). A one-step evaporation process (Figure 1b) over the same range of conditions leads to a defective swollen morphology. Because τ increases at higher ϕ_p, the annealing time becomes insufficient to rearrange the system into an equilibrium morphology at larger ϕ_p with larger domain spacings, but it is enough to yield a well-ordered morphology that is initiated at a smaller ϕ_p during the first solvent evaporation step. The results presented here for two-step evaporation provide not only a viable strategy for defect reduction, one that could find widespread use in applications, but also offer the possibility of designing processes where the main objective is to trap metastable, nonequilibrium morphologies in the dried state.[45] The insights provided in this work into the preparation of nonequilibrium morphologies have the potential to greatly expand and diversify the range of possible applications of solvent-assisted, directed self-assembly of BCP thin films.

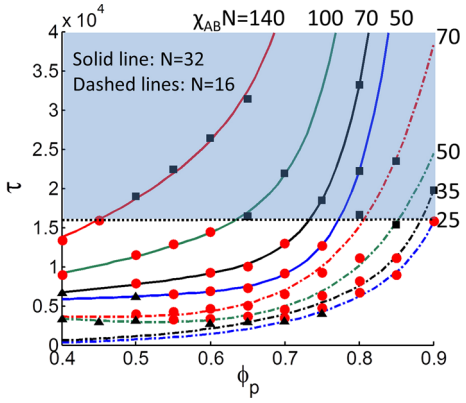

Figure 5. Defect annihilation time $\tau = \exp(0.025\chi_{eff}N)/D_0$ as a function of ϕ_p. Lines and symbols are the same as in Figure 4. A black horizontal dotted line is drawn at τ^* to delineate the minimum annealing time (or characteristic time for defect annihilation) beyond which defect-free structures are observed.

■ ASSOCIATED CONTENT

Ⓢ Supporting Information

Detailed model description and parameters are provided. This material is available free of charge via the Internet at http://pubs.acs.org.

■ AUTHOR INFORMATION

Corresponding Author

*E-mail: depablo@uchicago.edu.

Notes

The authors declare no competing financial interest.

■ ACKNOWLEDGMENTS

This work is supported by the U.S. Department of Energy, Office of Science, Office of Basic Energy Sciences-Materials Science. Additional support by the Semiconductor Research Corporation for development of fast simulation codes is gratefully acknowledged. M.M. received financial support by the European Union FP7 under Grant Agreement 619793 CoLiSA.MMP. We are grateful for valuable computing resources provided on Blues, a high-performance computing cluster operated by the Laboratory Computing Resource

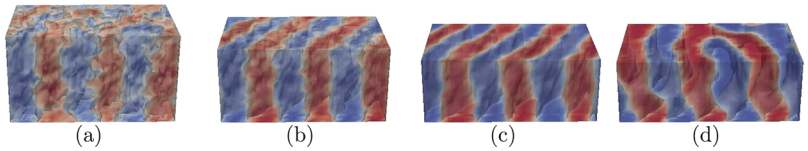

Figure 6. Self-assembly of symmetric BCP thin films of $\chi_{AB}N = 50$ after partial removal of solvent particles from a disordered swollen film ($\phi_p = 0.5$ as in Figure 1e). Films are exposed to various solvent pressures. The resulting ϕ_p are different ($\phi_p = 0.6$, 0.7, 0.8, and 0.9 for (a), (b), (c), and (d), respectively).

Center at Argonne National Laboratory, for resources provided by the Midway Research Computing Center at the University of Chicago, and by an INCITE Award at Argonne National Laboratory.

REFERENCES

(1) Albert, J. N.; Epps, T. H., III *Mater. Today* **2010**, *13*, 24−33.
(2) Kim, H.-C.; Park, S.-M.; Hinsberg, W. D. *Chem. Rev.* **2010**, *110*, 146−177.
(3) Welander, A. M.; Kang, H.; Stuen, K. O.; Solak, H. H.; Müller, M.; de Pablo, J. J.; Nealey, P. F. *Macromolecules* **2008**, *41*, 2759−2761.
(4) Jung, Y. S.; Ross, C. A. *Adv. Mater.* **2009**, *21*, 2540−2545.
(5) Jung, Y. S.; Chang, J. B.; Verploegen, E.; Berggren, K. K.; Ross, C. A. *Nano Lett.* **2010**, *10*, 1000−1005.
(6) Son, J. G.; Chang, J.-B.; Berggren, K. K.; Ross, C. A. *Nano Lett.* **2011**, *11*, 5079−5084.
(7) Gotrik, K. W.; Hannon, A. F.; Son, J. G.; Keller, B.; Alexander-Katz, A.; Ross, C. A. *ACS Nano* **2012**, *6*, 8052−8059.
(8) Paik, M. Y.; Bosworth, J. K.; Smilges, D.-M.; Schwartz, E. L.; Andre, X.; Ober, C. K. *Macromolecules* **2010**, *43*, 4253−4260.
(9) Bosworth, J. K.; Paik, M. Y.; Ruiz, R.; Schwartz, E. L.; Huang, J. Q.; Ko, A. W.; Smilgies, D.-M.; Black, C. T.; Ober, C. K. *ACS Nano* **2008**, *2*, 1396−1402.
(10) Kim, S. H.; Misner, M. J.; Xu, T.; Kimura, M.; Russell, T. P. *Adv. Mater.* **2004**, *16*, 226−231.
(11) Campbell, I. P.; He, C.; Stoykovich, M. P. *ACS Macro Lett.* **2013**, *2*, 918−923.
(12) Angelescu, D. E.; Waller, J. H.; Adamson, D. H.; Deshpande, P.; Chou, S. Y.; Register, R. A.; Chaikin, P. M. *Adv. Mater.* **2004**, *16*, 1736−1740.
(13) Marencic, A. P.; Chaikin, P. M.; Register, R. A. *Phys. Rev. E* **2012**, *86*, 021507.
(14) Sinturel, C.; Vayer, M.; Morris, M.; Hillmyer, M. A. *Macromolecules* **2013**, *46*, 5399−5415.
(15) Takahashi, H.; Laachi, N.; Delaney, K. T.; Hur, S.-M.; Weinheimer, C. J.; Shykind, D.; Fredrickson, G. H. *Macromolecules* **2012**, *45*, 6253−6265.
(16) Nagpal, U.; Müller, M.; Nealey, P. F.; de Pablo, J. J. *ACS Macro Lett.* **2012**, *1*, 418−422.
(17) Rudov, A. A.; Patyukova, E. S.; Neratova, I. V.; Khalatur, P. G.; Posselt, D.; Papadakis, C. M.; Potemkin, I. I. *Macromolecules* **2013**, *46*, 5786−5795.
(18) Paradiso, S. P.; Delaney, K. T.; Garca-Cervera, C. J.; Ceniceros, H. D.; Fredrickson, G. H. *ACS Macro Lett.* **2013**, 16−20.
(19) Detcheverry, F. A.; Pike, D. Q.; Nealey, P. F.; Müller, M.; de Pablo, J. J. *Phys. Rev. Lett.* **2009**, *102*, 197801.
(20) Detcheverry, F. A.; Pike, D. Q.; Nagpal, U.; Nealey, P. F.; de Pablo, J. J. *Soft Matter* **2009**, *5*, 4858−4865.
(21) Detcheverry, F. A.; Liu, G.; Nealey, P. F.; de Pablo, J. J. *Macromolecules* **2010**, *43*, 3446−3454.
(22) Hömberg, M.; Müller, M. *J. Chem. Phys.* **2010**, *132*, 155104−155104−18.
(23) Müller, M.; Smith, G. D. *J. Polym. Sci., Part B: Polym. Phys.* **2005**, *43*, 934−958.
(24) When the solvent evaporation is much slower than this, polymer chains have sufficient time to rearrange during the evaporation period, leading to morphologies with different domain sizes and defectivity. For concreteness, however, in this first study on solvent annealing, we focus on fast solvent evaporation.
(25) Helfand, E.; Tagami, Y. *J. Chem. Phys.* **1972**, *56*, 3592−3601.
(26) Naughton, J. R.; Matsen, M. W. *Macromolecules* **2002**, *35*, 5688−5696.
(27) Lodge, T. P.; Pan, C.; Jin, X.; Liu, Z.; Zhao, J.; Maurer, W. W.; Bates, F. S. *J. Polym. Sci., Part B: Polym. Phys.* **1995**, *33*, 2289−2293.
(28) Lodge, T. P.; Hanley, K. J.; Pudil, B.; Alahapperuma, V. *Macromolecules* **2003**, *36*, 816−822.
(29) Hanley, K. J.; Lodge, T. P.; Huang, C.-I. *Macromolecules* **2000**, *33*, 5918−5931.
(30) Joanny, J. F.; Leibler, L.; Ball, R. *J. Chem. Phys.* **1984**, *81*, 4640−4656.
(31) Fredrickson, G. H.; Leibler, L. *Macromolecules* **1989**, *22*, 1238−1250.
(32) Olvera de la Cruz, M. *J. Chem. Phys.* **1989**, *90*, 1995−2002.
(33) Guenza, M.; Schweizer, K. S. *Macromolecules* **1997**, *30*, 4205−4219.
(34) Huang, C.-I.; Lodge, T. P. *Macromolecules* **1998**, *31*, 3556−3565.
(35) Lodge, T. P.; Pudil, B.; Hanley, K. J. *Macromolecules* **2002**, *35*, 4707−4717.
(36) Xu, J.; Ma, Y.; Hu, W.; Rehahn, M.; Reiter, G. *Nat. Mater.* **2009**, *8*, 348−353.
(37) Blundell, D. J.; Keller, A.; Kovacs, A. J. *J. Polym. Sci., Part B: Polym. Lett.* **1966**, *4*, 481−486.
(38) Gu, X.; Gunkel, I.; Hexemer, A.; Gu, W.; Russell, T. P. *Adv. Mater.* **2014**, *26*, 273−281.
(39) Müller, M.; Binder, K.; Schäfer, L. *Macromolecules* **2000**, *33*, 4568−4580.
(40) Leibler, L. *Macromolecules* **1980**, *13*, 1602−1617.
(41) Fredrickson, G. H.; Helfand, E. *J. Chem. Phys.* **1987**, *87*, 697−705.
(42) Mishra, V.; Fredrickson, G. H.; Kramer, E. J. *ACS Nano* **2012**, *6*, 2629−2641.
(43) Lodge, T. P.; Dalvi, M. C. *Phys. Rev. Lett.* **1995**, *75*, 657−660.
(44) A "defect-free" structure is defined as one in which all the lamellar domains are completely uninterrupted, without any bridges or connections between domains. In contrast, "defective" structures exhibit interrupted lamellae.
(45) Müller, M.; Sun, D.-W. *Phys. Rev. Lett.* **2013**, *111*, 267801.